https://doi.org/10.1002/9783527636280.ch4

4
Capacitance Spectroscopy of Thin-Film Solar Cells

Jennifer Heath and Pawel Zabierowski

4.1
Introduction

Capacitance or, more generally, admittance measurements are particularly suited for probing bulk and interface properties of a buried layer in a working diode-like device, such as a solar cell. The small signal capacitance is by definition sensitive to carrier capture and emission from trap states, being the charge response δQ to a small change of voltage δV, $C = \delta Q/\delta V$. A number of experimental techniques have been developed to exploit this sensitivity and try to map out the sub-bandgap density of states, with the most broadly applied being capacitance–voltage (CV) profiling, admittance spectroscopy (AS), and deep level transient spectroscopy (DLTS). In addition to these, we will also discuss drive level capacitance profiling (DLCP) and photocapacitance techniques. In this chapter, we endeavor to introduce these techniques from introductory concepts, while also commenting on the analysis of data from real photovoltaic materials, which is definitely an advanced topic. Although it is not possible to cover every scenario, we try to give examples, as well as references to a wide range of resources.

The electronic states associated with defects and impurities are typically divided into two broad categories: "shallow" and "deep" states, corresponding, respectively, to centers with extended electronic wavefunctions, and those that are strongly localized [1]. Generally speaking, the techniques discussed here are designed to detect nonradiative transitions involving deep states. Deep states act as traps and recombination centers, reducing the minority carrier mobility, and in some cases pinning the Fermi energy deep in the gap. The electrical activity and even the physical nature of deep states can be complex. Quite energetically shallow states can also be observed in photocapacitance measurements as a valence (or conduction) bandtail; these disorder-induced traps reduce the drift mobility.

Much effort has gone into extending junction capacitance techniques to accurately measure properties of the more continuous densities of sub-bandgap states characteristic of imperfect materials. This includes early work by Losee [2] to treat generally the effect of gap states on admittance in Schottky devices as well as

Advanced Characterization Techniques for Thin Film Solar Cells,
Edited by Daniel Abou-Ras, Thomas Kirchartz and Uwe Rau.

experimental and numerical studies by Cohen and Lang [3, 4] to treat the case of continuous densities of states. In-depth discussions of the field are provided by Refs. [5, 6].

Admittance measurements generally begin with a simple CV evaluation of the diode, including whether significant shunt current exists, whether the film is fully depleted, and a rough estimate of doping density. For suitable devices, AS or DLTS data directly give the thermal trapping time of gap states, while DLTS or other transient measurements indicate whether these are majority or minority carrier traps. We will discuss ways in which additional information can also be gleaned from capacitance data, including the energetic position, density and spatial variation of the defect transition; the carrier capture cross section; and, in some cases, the position of the Fermi energy. The photocapacitance techniques measure optical transitions involving defect states, and are particularly valuable for studying optical properties of the buried absorber layers in working photovoltaic devices. The relationship between optical and thermal transition energies can also lead to a better understanding of lattice relaxation effects.

4.2 Admittance Basics

This chapter makes use of the differential capacitance, $C = \delta Q/\delta V$, as opposed to the dc capacitance definition more commonly used in circuits, $C = Q/V$. These two definitions converge for standard capacitors. The differential capacitance describes the physical quantity measured in capacitance spectroscopy and applies to a more general situation where Q may not vary linearly with V; in diodes we approximate $Q \propto \sqrt{V_{bi} - V}$ where V_{bi} is the built-in potential at the interface. However, in the small signal approximation we can still write $\delta Q \propto \delta V$.

When a small ac voltage is applied to a sample, the linear current response can consist of both a component in phase with the applied voltage, and a component that is 90° out of phase. We can represent the applied voltage V with amplitude V_{ac} and angular frequency ω as a function of time t

$$V = V_{ac}\exp(j\omega t) = V_{ac}[\cos(\omega t) + j\sin(\omega t)]$$

For the ideal resistor, R, and capacitor, C, in parallel, we measure a total current, I

$$I = V(R^{-1} + j\omega C)$$

Note that information about the resistor and capacitor values are clearly separated into the real and imaginary parts of the current, and hence the admittance.

This current can be represented using a phasor diagram on the complex plane, as illustrated in Figure 4.1a and b, and analogous diagrams can be used to represent various types of data, including the voltage difference between two measurement points, and the impedance or admittance of the circuit element. The amplitude and phase of the phasor represent the measurement at time $t = 0$; the entire measure-

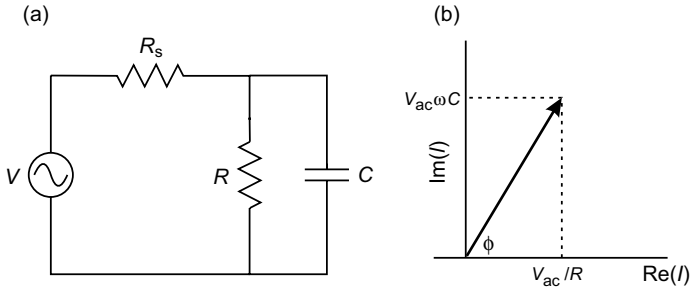

Figure 4.1 (a) Parallel circuit model for the device, with series resistor. (b) Phasor diagram for (a), neglecting R_s.

ment as a function of time corresponds to the real component of the phasor as it rotates counter-clockwise with angular velocity ω.

The small signal response of any sample can be characterized by its complex admittance, $Y = Y' + jY''$, such that $I = YV$, where Y' is the conductance, and Y'' is the susceptance. The complex impedance, $Z = Z' + jZ''$, is the inverse of admittance, such that $V = IZ$. Here, Z' is the resistance, and Z'' is the reactance. Here, we focus on admittance measurements, since the complex admittance normally allows the diode capacitance to be clearly separated from the shunt conductance.

For diodes, including solar cell devices, we frequently assume a simple parallel circuit model, as illustrated in Figure 4.1a and b, such that $C = Y''/\omega$. The most common complication is a too-high series resistance or frequency, such that either the condition $\omega R_s C \ll 1$ or $R_s \ll R$ is violated; in this case the series resistance and capacitance essentially form a low-pass filter, and as ω increases, Y''/ω no longer accurately yields C. This issue can originate either from resistance in the device and contacts, or from spreading resistance in the contact and film. Series resistance can be estimated from the dc current–voltage curve at forward bias, and its influence on the data can additionally be checked by intentionally adding a resistor in series with the device. Problems with spreading resistance can be mitigated by reducing the device area; however, this can in some cases increase the influence of stray capacitance from the edges of the device. Assuming a simple model, as illustrated in Figure 4.1a and b, with a frequency independent series resistance, a peak in the Y'/ω versus ω curve will be observed at $\omega R_s C = 1$, and as ω continues to increase, the apparent capacitance, Y''/ω, will decrease as ω^{-2}. At high frequencies, stray inductance may also be a complicating issue. A more complete discussion of dielectric response than is possible here is found in Ref. [7].

4.3 Sample Requirements

In general, any diode-like devices, including working solar cells, can be studied using the techniques described here. Of course, the diode quality must permit the

capacitive response from the space charge region to be clearly distinguished. For simplicity, in this chapter we generally assume a single junction, either a one-sided p^+–n or n^+–p, or Schottky device in which the lightly doped semiconductor is not fully depleted. The treatment discussed here is also consistent for MOS devices as long as they are measured in the depletion regime. Since the oxide is in series with the semiconductor, its effect on the capacitance can easily be subtracted. Interface states also contribute more strongly to the capacitance response in MOS devices, as discussed more below; this can either be a complication or an opportunity. In-depth treatments of the theory appropriate to these more complex device structures are provided elsewhere [5, 8]. Other multilayer devices, including p–i–n structures, can also be studied. In such devices, definitively tying experimental observations to a particular layer or interface of the device becomes more complicated.

In thin-film devices, the reproducibility of sample characteristics and measurement results has been problematic. Sensitivities to light, voltage, temperature, humidity, oxygen, etc., are well documented. In addition, comparisons between samples grown in different labs must be undertaken with caution.

4.4 Instrumentation

To measure admittance, the small ac current response to an applied ac voltage must be measured. This signal consists of two parts: the amplitude and phase. Equivalently, it can be decomposed into components corresponding to the in-phase current and the current that is 90° out of phase. Many LCR meters (impedance analyzers) will directly provide this measurement. Alternatively, a more affordable option is to employ a lock-in amplifier and trans-impedance amplifier (current-to-voltage preamplifier) together to perform the same function, as illustrated in Figure 4.2. The ability to vary the ac frequency is essential. Generally, it is also important to control the ac voltage amplitude and apply a dc voltage offset.

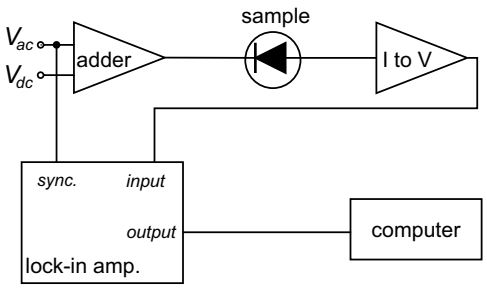

Figure 4.2 Schematic for a lock-in amplifier-based approach to measurement of complex admittance.

In the case where transient signals must be evaluated, for example, after a voltage pulse, several approaches exist. The LCR or lock-in amplifier output can be displayed on an oscilloscope, or collected directly by a data acquisition card and specialized software. In either case, the speed, accuracy, and timing or triggering of the digital data acquisition are essential considerations. The entire transient can be collected and stored for future analysis; collecting the data on a logarithmic time scale allows both short- and long-term contributions to the transient to be analyzed. This may be preferred for measurements of thin-film devices, allowing unusual behavior to be recognized, and allowing the flexibility to attempt different analyses. The analysis of exponential transient signals is discussed by Istratov and Vyvenko [9]. Some purpose-made DLTS equipment uses the Fourier transform approach discussed therein.

Regardless of the admittance measurement approach, careful calibration is required at each measurement frequency. Measurements at higher frequencies, above about 1 MHz, require extra attention to circuit components, connections, and calibration [10].

During the measurement, it is critical to monitor the relationship between conductance and susceptance, characterized by either the quality factor, Q, or dissipation factor D. These factors are defined such that $Q = D^{-1} = Y''/Y = \tan(\phi)$, where ϕ is illustrated in Figure 4.1b. Typically, D should be less than $\sim$10. When D is large, such as for large leakage currents or low measurement frequencies, small errors in the measurement of ϕ can lead to large errors in determining Y'' and therefore C. It is straightforward to test the sensitivity and calibration of instrumentation with RC circuits constructed of known components.

In addition to the measurement of capacitance, sample temperature generally must be varied. The required temperature range will depend on the sample, with lower temperatures allowing measurement of transitions from shallower states, but most authors find that an l-N_2 cryostat suffices. The importance of accurately measuring the stabilized sample temperature cannot be overemphasized as it directly influences the accuracy of parameter extraction. It is advisable to carefully consider the temperature sensor and location, calibration, and optimal thermal design of the sensor–sample–cryostat system. For example, thin films grown on glass and placed in a cold-finger-type cryostat in vacuum can lag the cold-finger temperature significantly.

4.5
Capacitance–Voltage Profiling and the Depletion Approximation

The diode capacitance is traditionally analyzed using the depletion approximation. Although this approximation may not be very accurate for thin-film semiconductors, which can have significant densities of deep states, it is still a useful starting point for this discussion of admittance measurements. The depletion approximation assumes that the depletion region is precisely defined, ends abruptly, and is fully depleted of free carriers. In the depletion approximation, the depletion width will vary with applied bias, but the charge density $\rho(x)$ within the depleted region remains constant

(where x is measured through the depth of the film, with $x = 0$ at the interface), while the bulk region remains neutral. Then, as long as the free carrier relaxation time is short compared with the applied ac frequency, the capacitance response originates from the depletion edge, giving $C = \varepsilon\varepsilon_0 A/W$, where W is the width of the depletion region, A is the area of the device, and ε is the semiconductor dielectric constant.

For an abrupt, one-sided junction or Schottky junction

$$W = \sqrt{\frac{2\varepsilon\varepsilon_0(V_{bi} - V_{dc})}{eN_B}}$$

where N_B is the doping concentration on the lightly doped side of the junction, e is the elementary charge, and V_{dc} is the applied dc bias, where V_{dc} is positive for forward bias [11]. Then

$$C^{-2} = \frac{2(V_{bi} - V_{dc})}{e\varepsilon\varepsilon_0 A^2 N_B}$$

So in a plot of C^{-2} versus V_{dc}, the intercept gives V_{bi}, and the slope yields the CV density, N_{CV}, which in this ideal situation is identical to N_B

$$N_{CV} = -\frac{2}{e\varepsilon\varepsilon_0 A^2}\left[\frac{d(C^{-2})}{dV_{dc}}\right]^{-1} = -\frac{C^3}{q\varepsilon\varepsilon_0 A^2}\left(\frac{dC}{dV_{dc}}\right)^{-1} \tag{4.1}$$

Since, in the depletion approximation, the capacitance response originates solely from the edge of the depletion region, this result also holds true when N_B varies with position, x, through the thickness of the semiconductor [12]. So, $N_B(x)$ can be found using Eq. (4.1), where $x = \varepsilon\varepsilon_0 A/C$ is measured from the junction.

Measurement of $C(V)$ can thus give a one-dimensional profile of the doping density N_B as a function of position through the thickness of the semiconductor, with a spatial resolution characterized by the Debye screening length L_D [13]. The parabolic band bending changes by kT/e over a distance of L_D, where $L_D = \sqrt{\varepsilon\varepsilon_0 kTe^{-2}N_B^{-1}}$. To neglect the transition region at the depletion edge, we require $W \gg L_D$.

In crystalline materials, capacitance measurements as a function of voltage (CV) are considered a straightforward method to profile $N_B(x)$. However, the relatively large density of deep states in thin-film semiconductors can make it impossible to find the free carrier density using CV, as further discussed in Section 4.7.

4.6 Admittance Response of Deep States

When energy levels are present deeper in the band gap, then the depletion approximation no longer necessarily holds true, and carrier capture and emission from these states must also be considered.

The electron capture rate, c_n, into an unoccupied state is

$$c_n = \sigma_n \langle v_n \rangle n$$

where σ_n is the capture cross section for electrons, and n is the density of free electrons moving with rms thermal velocity $\langle v_n \rangle$,

$$n = N_c \exp\left(-\frac{E_C - E_F}{kT}\right)$$

The principle of detailed balance states that in thermal equilibrium, the capture and emission of electrons must be equal, and similarly the capture and emission of holes must balance. For electrons, this gives

$$e_n n_T = c_n (N_T - n_T)$$

where e_n is the emission rate of electrons, N_T is the total density of electron traps, and n_T is the density of occupied traps. Therefore, the fractional occupancy of the trap in thermal equilibrium, which is also given by the Fermi–Dirac distribution function, can be used to relate the capture and emission times to the energetic position of the trap

$$\frac{n_T}{N_T} = \frac{c_n}{c_n + e_n} = \left[1 + \frac{g_0}{g_1}\left(\frac{E_T - E_F}{kT}\right)\right]^{-1}$$

This then gives the emission rate as

$$e_n = \sigma_n \langle v_n \rangle N_c \frac{g_0}{g_1} \exp\left(-\frac{E_c - E_T}{kT}\right)$$

where g_0 and g_1 represent the degeneracy of the initial and final states, respectively.

Since these values, particularly σ_n and E_T, may themselves depend on temperature, they can differ from the measured (apparent) capture cross section σ_{na} and thermal activation energy E_{na} of the trap determined from the thermally activated experimental data. This temperature dependence can have multiple origins. For deep states, a transition corresponds to a change from one charge state to another, so it is common for deep states to be charged, and therefore attractive or repulsive. Deep states may also reside in a larger, local concentration of traps that has an overall net charge and modifies the local free carrier density [14, 15]. Additionally, the change in entropy with the change in trap state occupation may play a role as discussed in Section 4.13.

Electron emission from the defect is thus a thermally activated process with

$$e_n = \gamma \sigma_{na} T^2 \exp\left(-\frac{E_{na}}{kT}\right) \tag{4.2}$$

where, since we can approximate $N_c \propto T^{3/2}$ and $\langle v_n \rangle \propto T^{1/2}$, the temperature dependence of $N_c \langle v_n \rangle$ is isolated by defining $\gamma = N_c \langle v_n \rangle T^{-2}$ (assuming no temperature dependence of σ_{na}). For hole traps, Eq. (4.2) has the identical form, with E_{pa} referenced to the valence instead of the conduction band edge.

This model assumes that the density of deep states obeys the principle of superposition, such that each deep state creates a set of discrete electronic energy

transitions that can be added together to give the total density of states within the band gap; interactions between states are neglected. Then, broad densities of states may originate from a single type of defect that is in a variety of different local environments. In real films, deep states can also interact with each other and with the lattice in complex ways that shift and broaden the density of states, and can result in changes in the defect configuration or even diffusion of the trap center upon capture or emission of carriers (see, e.g., [16, 17]).

The differential capacitance of the sample originates from its response to a small voltage perturbation, δV. In the small signal approximation, $\delta V < kT/e$. (Typical values of V_{ac}, around 30 mV, do not strictly satisfy this requirement, which may slightly impact the data [18, 19].) The resulting change in the band bending causes a change in trap state occupation at the location, x_T, where E_T is within kT of E_F, as illustrated in Figure 4.3. Thus, traps contribute to the capacitance in two ways: (i) Traps modify the space charge density and therefore the depletion width W, and (ii) in the vicinity of x_T, the traps may be able to change their charge state dynamically, following the ac voltage, and contributing to $\delta Q/\delta V$.

The characteristic time of the capacitance measurement is defined by the angular frequency of the applied ac voltage, ω, such that states with emission rates $e_n > \omega$

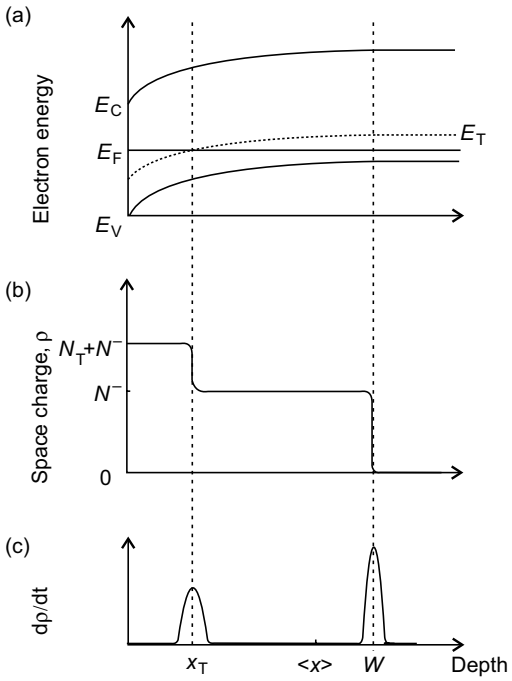

Figure 4.3 (a) Schematic of band bending with one deep trap state. (b) Charge density variation through the depletion region due to the trap state; same scale as (a). (c) In response to a changing bias, dV/dt, changes in space charge density $d\rho/dt$ can occur at both x_T and W, as indicated.

respond to V_{ac}.[1] By rewriting Eq. (4.2), we can see that only states with apparent activation energies E_{na} up to the demarcation energy, E_e, will respond dynamically to the ac voltage, where

$$E_e = kT\ln\left(\frac{\gamma\sigma_{na}T^2}{\omega}\right) \tag{4.3}$$

Note that the demarcation energy depends on characteristics of the trap being measured, and so can be difficult to accurately determine; the same ω, T may probe different energies for physically different traps.

A general expression for the capacitance of the diode, which does not assume any specific density of states in the gap, can be derived starting from the identity

$$\frac{d}{dx}\left(x\frac{d\psi}{dx}\right) = \frac{d\psi}{dx} - x\frac{\rho}{\varepsilon\varepsilon_0}$$

where x is measured through the depth of the semiconductor ($x = 0$ at the interface), $\rho(x)$ is the depletion charge density, and $\psi(x)$ is the position-dependent potential in the depletion region, and is defined to be zero far from the interface, such that $\psi(\infty) = 0$ and $d\psi/dx\ (\infty) = 0$. Then

$$\int_0^\infty \frac{d}{dx}\left(x\frac{d\psi}{dx}\right)dx = 0 = \int_0^\infty \frac{d\psi}{dx}dx - \int_0^\infty x\frac{\rho}{\varepsilon\varepsilon_0}dx$$

and the value of ψ can be written as an integral over the charge density

$$\psi(0) = -\int_0^\infty x\frac{\rho}{\varepsilon\varepsilon_0}\,dx$$

Application of a small voltage, δV, is equivalent to a voltage change at the interface of $-\delta V(0)$ since $\psi(0) = V_{bi} - V_a$, where V_{bi} is the built-in potential and V_a is the voltage applied across the junction. The charge response is $\delta Q = A\int_0^\infty \delta\rho(x)\,dx$, where $\delta\rho$ is the change in charge density due to δV, and A is the area of the contact. Now the capacitance is

$$C = \frac{\varepsilon\varepsilon_0 A\int_0^\infty \delta\rho(x)\,dx}{\int_0^\infty x\delta\rho(x)\,dx} = \frac{\varepsilon\varepsilon_0 A}{\langle x\rangle} \tag{4.4}$$

where $\langle x\rangle$ is the first moment of charge response, also called the center of gravity of the charge response.

1) A better approximation in a depletion region dominated by a single deep trap level requires $f_t > \omega$, where $f_t = 2e_n\left(1 + \frac{x_t N_t}{WN_B}\right)$ [5].

Assumptions about the trap occupation and its response to ac and dc bias (and hence, its effect on $\langle x \rangle$) form the foundation of all the techniques discussed here. In both CV and DLTS, it is assumed that the frequency is chosen such that $\omega > e_{n,p}$ for any deep traps; then, they do not respond dynamically to the ac bias, and $\langle x \rangle = W$. In CV it is also assumed that deep traps either do not change their charge state with the dc bias, or are few enough not to have a significant influence on W. In contrast, in DLTS, the dc bias on the sample is assumed to have a strong effect on the trap state occupation. Indeed, the change in occupation of the traps in response to the dc bias yields the DLTS signal, as is further discussed in Section 4.8. In AS and DLCP, the ac frequency and/or the temperature are varied to ramp ω from values below $e_{n,p}$ to above $e_{n,p}$.

4.7
The Influence of Deep States on CV Profiles

Even if trap states do not respond to the ac voltage they may adjust their charge state to the dc bias conditions, which results in artifacts in the CV profiles. To illustrate this behavior we consider a SCAPS1D simulation of the $n^+ - p$ junction containing uniform distributions of shallow and deep ($E_T = E_V + 0.3\,\text{eV}$) acceptors of the concentrations $N_A = 2 \times 10^{15}\,\text{cm}^{-3}$ and $N_T = 2 \times 10^{16}\,\text{cm}^{-3}$, respectively [20, 21]. Figure 4.4a displays $N_{CV}(\langle x \rangle)$, where N_{CV} and $\langle x \rangle$ are determined according to Eqs. (4.1) and (4.4), respectively. These values are simulated at two measurement frequencies: $\omega_L < e_p$ and $\omega_H > e_p$. In this simulation, the deep traps are assumed to be in equilibrium with the dc bias (similar to Figure 4.3). Then, the shallow acceptor density N_A is not reproduced at either frequency. At ω_L, $N_{CV} = N_A + N_T$ is measured, while at ω_H, N_{CV} is a function of V_{dc}, with $N_A \leq N_{CV} \leq N_A + N_T$, since the static charge accumulated at deep states follows the dc voltage sweep and influences the

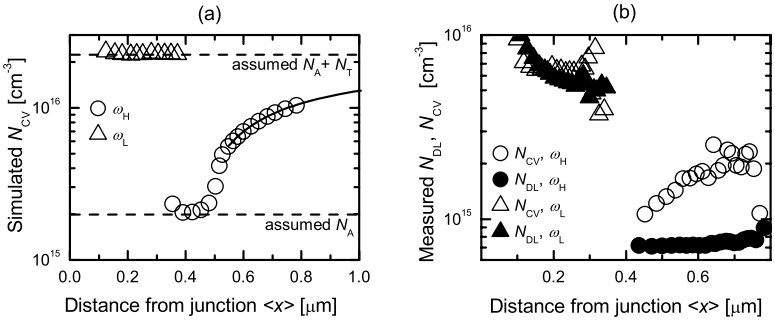

Figure 4.4 (a) Simulated CV profiles at two frequencies: low (ω_L, open triangles) and high (ω_H, open circles) as described in the text. The solid line is a fit using Eq. (4.5). Best-fit parameters are identical to assumed values of N_A and N_T, and yield $\lambda = 0.45$. (b) Experimental CV (open symbols) and DLCP (closed symbols) data for a $CuInSe_2$ device. Device details are described elsewhere [67]. All data were collected at 11 kHz, which corresponds to a low frequency at 280 K (triangles), and a high frequency at 180 K (circles).

capacitance. In this case the charge distribution delivered by CV profiling can be approximated by [22]

$$N_{CV} = N_T(x_T)[1-\lambda/W] + N_A(W) \tag{4.5}$$

where $\lambda = W - x_T$ is assumed to remain constant for applied dc voltages.

Thus, when trap densities are significant, the CV profile does not clearly yield the densities N_A and N_T nor indicate their uniformity. As discussed in Section 4.10 and illustrated in Figure 4.4a and b, DLCP can help sort out these issues. A longer discussion on the influence of deep states, including interface states, on CV and DLCP measurements, can be found in [23].

4.8 DLTS

In the standard approach, DLTS analysis consists of extracting the emission rates of deep levels from a transient capacitance signal, as illustrated in Figure 4.5a–c [23].

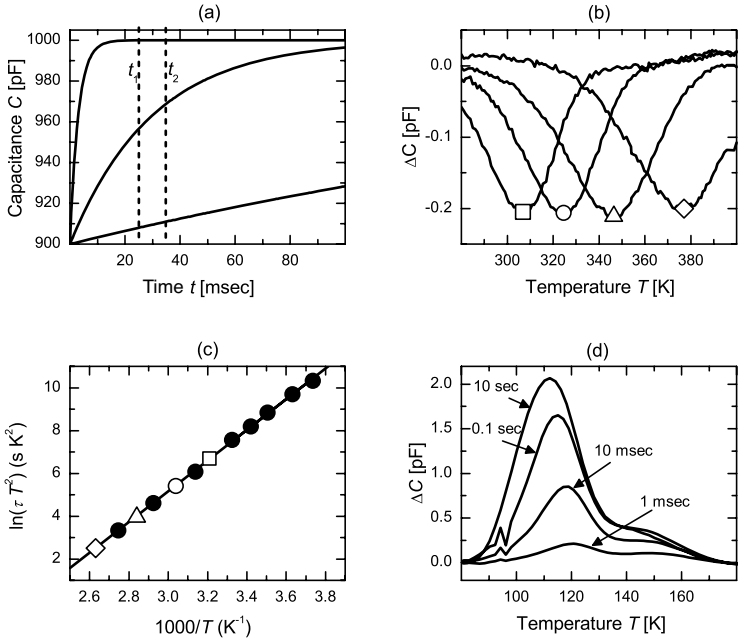

Figure 4.5 (a) Schematic transients. The DLTS signal, $[C(t_1) - C(t_2)]/C_0$, will be maximized when the rate window and emission rate match (Eq. (4.11)). (b) DLTS data for a GaAsN device. Each trace corresponds to a different rate window. (c) Arrhenius plot yielding E_{na} and σ_{na} of the trap. Data points corresponding to peaks in (b) are indicated with the same symbol. (d) Filling pulse dependence of the DLTS signal for the same sample; in this case data for a minority carrier trap is shown. The labels indicate filling pulse length. See [68, 69] for further discussion. Data courtesy of Steve Johnston, National Renewable Energy Laboratory.

These transients result from a voltage or optical pulse applied to the junction. In its simplest application, DLTS allows for determination of deep trap parameters such as the type of the defect (majority or minority carrier trap), activation energy, capture cross sections, and trap concentration.

To understand the DLTS signal, we are interested in calculating how a change of a charge ΔQ at some distance x from the interface ($x = 0$) will influence the junction capacitance. It is assumed that the additional charge is trapped at defect states of the concentration N_T within a layer of the width Δx. Hence, $|\Delta Q| = q\Delta x N_T$. If we do not initially assume a one-sided junction, then this charge will induce a change of the depletion layer width $\Delta W = \Delta W_n + \Delta W_p$, where ΔW_n and ΔW_p are the depletion widths on the n and p side of the junction, respectively. Small capacitance changes ($\Delta C \ll C$) can be approximated as

$$\frac{\Delta C}{C} \approx -\frac{\Delta W}{W} \tag{4.6}$$

By solving the Poisson equation, ΔW can be eliminated from Eq. (4.6) yielding [24]

$$\frac{\Delta C}{C} \approx \mp \frac{N_T \Delta x}{W^2}\left(\frac{x + W_n}{N^-} - \frac{W_p - x}{N^+}\right) \tag{4.7}$$

where N^+ and N^- are the densities of ionized space charge on the n and p sides of the junction, respectively. The negative and positive signs correspond to decrease and increase of negative charge, respectively, or equivalently, an increase and decrease of positive charge. Rewriting Eq. (4.7) for a spatial distribution of trapping states within the depletion layer yields

$$\frac{\Delta C}{C} \approx \mp \int_{-W_n}^{W_p} \frac{N_T(x)}{W^2}\left(\frac{x + W_n}{N^-} - \frac{W_p - x}{N^+}\right) dx \tag{4.8}$$

For highly asymmetrical junctions, (here n^+–p), assuming a uniform defect distribution, and neglecting the transition region, one arrives at

$$\frac{\Delta C}{C} \approx \mp \frac{N_T}{2N^-} \tag{4.9}$$

Thus, by measuring the capacitance transient $\Delta C(t)$, one can easily monitor the occupation of deep levels while the system relaxes after the equilibrium has been disturbed, for example, by application of a voltage or a light pulse.

The above equations show that the sensitivity of the capacitance change depends on the location of the trapped charge within the junction: it is highest at the border of the space charge layer and decreases toward the interface. For $x = 0$, that is, if the charge is accumulated at the very interface, the capacitance does not change at all ($\Delta C = 0$), since by charge neutrality $N^+ W_n = N^- W_p$. For this reason, an MIS-type structure can be an advantage in studying interface states with DLTS. Equations (4.8) and (4.9) also hold true for an MIS diode, or for an n^+–i–p (p^+–i–n) structure, assuming the depletion width W_n (W_p) remains constant [25, 26].

Depending on the nature of the perturbing pulse and the characteristics of the trap states, the transient can be due predominately to either an emission or a capture of majority or minority carriers. In most materials, there may be many different trap states and, assuming as in the SRH model that they are noninteracting and have discrete energy levels, the capacitance transient will consist of a sum over many exponentials.

To observe the emission of majority carriers, the junction is initially maintained in quasiequilibrium at reverse bias $-U_R$. Majority carrier traps of the concentration N_T are ionized in a region of width $W(-U_R) = W_R$ and contribute to the junction capacitance $C(-U_R)$. During the bias pulse, the reverse bias voltage and therefore depletion width are reduced for a time t_p, and these traps capture free carriers that appear in the previously depleted region. When the reverse bias is restored, the excess free carriers will be swept away. However, the trapped majority carriers reduce the space charge density, increasing the depletion width and causing the capacitance to drop below $C(-U_R)$ by ΔC. These trapped carriers are thermally emitted, and the capacitance gradually increases back toward $C(-U_R)$. This will be observed as a capacitance transient.

In the depletion region there are practically no free carriers, and capture processes can be neglected [6]. For an n^+–p junction, assuming $e_p \gg e_n$, which usually holds for acceptor-type defects located in the lower part of the band gap, the capacitance transient $C(t)$ is characterized by a single time constant $\tau = 1/e_p$

$$C(t) = C_\infty \left[1 - \frac{N_T}{2N^-} \exp(-e_p t)\right]$$

where C_∞ is the quasiequilibrium capacitance, in this case equal to $C(-U_R)$. An analogous equation is obtained for a p^+–n junction.

In this kind of experiment, the charge state of minority carrier traps usually does not normally change during the pulse [27]. To investigate such defects it is necessary to inject minority carriers into the depletion region by forward biasing the junction during the pulse or applying an optical pulse. For positively charged donors in p-type material electron capture will prevail ($c_n \gg c_p$) and at the end of the pulse most of the traps will be occupied by electrons. Hence the negative space charge increases, which gives $\Delta C > 0$. After the pulse these electrons will be emitted and the charge relaxation results in a capacitance transient characterized by a single time constant $\tau = 1/e_n$

$$C(t) = C_\infty \left[1 + \frac{N_t}{2N^-} \exp(-e_n t)\right]$$

where N_t is the density of minority carrier (in this case, donor) traps in the material.

The sign of the capacitance transient $C(t)$ is always positive and negative for the emission of minority and majority carriers, respectively, independent of the conductivity type of the semiconductor (p or n). Note that significant series resistance can result in majority carrier traps appearing to have positive (minority carrier) transients. Apparent minority carrier transients should be checked by adding an

additional series resistor to the device and observing its influence on the sign of the transient [6].

The normalized DLTS signal is defined as the difference of the capacitance at times t_1 and t_2 ($t_1 < t_2$)

$$S(T) = \frac{C(t_1) - C(t_2)}{\Delta C(0)} \tag{4.10}$$

where $\Delta C(0)$ is the maximal capacitance change [24]. The $S(T)$ curve is called a DLTS spectrum. Since the emission rate[2] is an increasing function of temperature, $S(T) = 0$ for very slow (low T) and very fast (high T) transients. At intermediate temperatures $S(T)$ passes an extremum[3] as the time constant of the transient $\tau_{n,p}$ equals the rate window τ, defined as

$$\tau = \frac{t_1 - t_2}{\ln(t_1/t_2)} \tag{4.11}$$

Activation energy and capture cross section of investigated traps can be calculated from the slope and intercept of Arrhenius plot as illustrated in Figure 4.5c. The trap concentration can be evaluated using Eq. (4.9), provided the shallow net doping level is known.

4.8.1 DLTS of Thin-Film PV Devices

The above considerations were conducted under a number of simplifying assumptions, which very often are not fulfilled in thin-film PV devices. Typical complications that arise if one tries to apply the quoted standard formulae include:

1) In the so-called λ-effect, DLTS peak height is not related to deep trap concentration in a simple equation but depends on the energetic position of the defect level in the band gap. To derive the more accurate formula, $\Delta C/C \approx f_\lambda N_T/2N^-$, where f_λ is a function of trap occupancy, one has to take into account the distance λ between the depletion edge and the point where the trap level and the quasi-Fermi level intersect [28].
2) The approximation $\Delta C/C \approx -\Delta W/W$ breaks down when deep trap concentrations are large, which has severe consequences for the DLTS signal analysis: (i) the capacitance transients become nonexponential, which influences the shape of DLTS peaks, (ii) DLTS peak position, and thus calculated activation energy and capture cross section, start to depend on the N_T/N-ratio, and (iii) the λ-effect becomes more pronounced [29].
3) Since the emission of carriers occurs at large reverse biases, the emission rates can be influenced by the electrical field through Poole–Frenkel and tunneling

2) It is assumed that the response of a single level is observed. Ideally, different levels have significantly different emission rates, at a given temperature, and their responses can be clearly separated.

3) A maximum or a minimum occurs for minority and majority carrier traps, respectively.

effects [30, 31]. To avoid this kind of complication, reverse bias DLTS (RDLTS) mode is used [32].

4) If a few closely spaced energy levels contribute to the capacitance transient in the same temperature range, the poor resolution of the standard (R)DLTS method does not allow for a clear separation of the individual components. Application of an inverse Laplace transform to the analysis of capacitance transients, called the Laplace-DLTS method, increases the resolution by an order of magnitude [33, 34]. However, one has to be extremely careful while interpreting emission rate spectra since $s(e_p)$ is always a result of numerical calculations.
5) Nonexponential response, for example, due to defect relaxation, sometimes dominates capacitance transients and can be misinterpreted as the energetic distribution of defects within the band gap. This issue is closely related to metastable phenomena, discussed in Section 4.14.
6) Barriers to carrier capture may require a fairly long filling pulse to fully populate the traps, as illustrated in Figure 4.5d. The dependence of DLTS signal on pulse length can allow the capture barrier energy to be measured [5]. This behavior can also be confused with metastable changes in the device.

4.9 Admittance Spectroscopy

Measurement of the sample admittance as a function of applied ac frequency and temperature is termed AS. This technique can yield the thickness of the film, the position of the Fermi energy in the bulk, the energetic position of dominant defect bands that occur between the Fermi energy and mid-gap, and an estimate of the density of those states. In contrast to both the DLTS and CV techniques, in AS the frequency (or temperature) is ramped so as to cross the transition frequency where the traps just start to respond. Note that AS can only detect traps between the band edge and mid-gap [35].

When the sample is too cold, or the frequency too high, then there is no time for carriers in the bulk, undepleted material to shift in and out of the depletion edge in response to the applied voltage, and a condition called freeze-out occurs. Under these conditions, the capacitance response will be that of the bulk dielectric, $C = \varepsilon\varepsilon_0 A/h$, where h is the distance between the top and back contacts. Increasing the temperature, T, or decreasing the frequency, f, eventually a step will be observed from $C = \varepsilon\varepsilon_0 A/h$ to $C = \varepsilon\varepsilon_0 A/W$.

The dielectric relaxation time, τ_R, is determined by $\tau_R = \rho_s \varepsilon\varepsilon_0$. The resistivity of the semiconductor, ρ_s, depends on the free carrier density, which has a thermal activation energy of E_F, and the mobility. So, this initial step in the capacitance occurs at a characteristic energy of E_F as long as E_F does not vary strongly with T and the mobility is approximately constant. If the charge transfer is instead limited by mobility, usually seen at high frequencies, then these data may give the majority carrier mobility in the film [36].

As T continues to increase or f decrease, trap states can begin to respond. The demarcation energy E_e (Eq. (4.3)) determines the cut-off energy for trap response at a

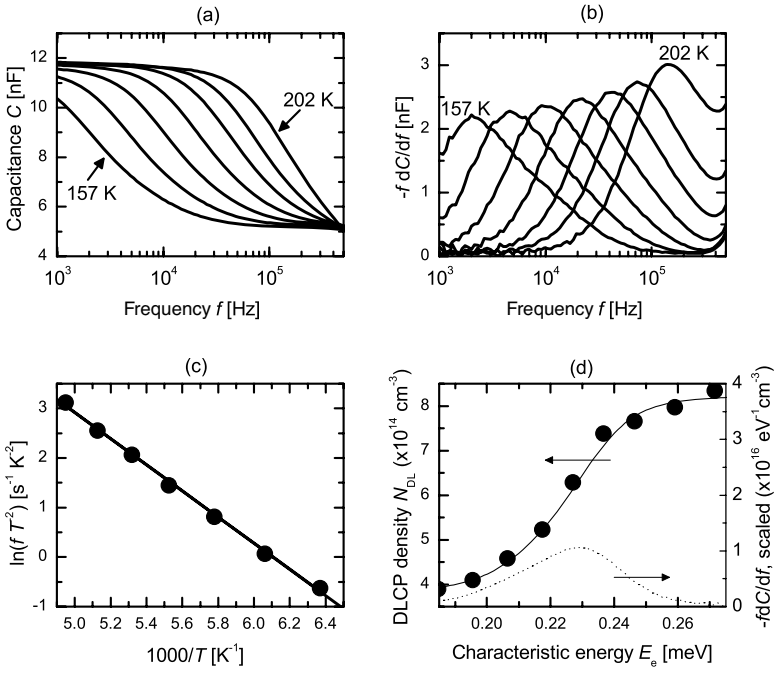

Figure 4.6 (a) Sample AS raw data, for a CIGS device. Data was taken in 8 K increments from 157 to 202 K. (b) The AS data after applying Eq. (4.12), showing the characteristic (peak) frequencies at each temperature. (c) Arrhenius plot of each peak (circles). A linear fit (line) yields $E_{na} = 0.23$ eV and $\gamma\sigma_{na} = 1.0 \times 10^7\ s^{-1}\,K^{-2}$. (d) DLCP data (circles), collected at 45 kHz, at the location $\langle x \rangle = 1.3$–$1.4\ \mu m$, and at temperatures ranging from 157 to 220 K. The integral over the 181 K AS ($-fdC/df$) data (solid line) was scaled by a constant factor to show the close agreement of transition energy and magnitude between AS and DLCP. The raw AS ($-fdC/df$) data at 181 K (dashed line), adjusted by the same scaling factor, thus represents the density of states for the 0.23 eV trap. Data courtesy of Jian V. Li, National Renewable Energy Laboratory.

certain T, f data point. When $E_T = E_e$, the occupation of the state can follow the ac voltage, and its charge state will change at the location x_e. This causes $\langle x \rangle$ to move closer to the interface and C to increase from $\varepsilon\varepsilon_0 A/W$ to $\varepsilon\varepsilon_0 A/\langle x \rangle$ as shown in Figure 4.6a. Successively deeper trap states respond as E_e is further increased.

Steps in C correspond to peaks in G/ω, due to their causal relationship. This correspondence can be calculated using the Kramers–Kronig transformations, which relate the real and imaginary parts of the susceptibility, χ' and χ'', respectively [7]. A slight correction may be necessary to apply these transformations within the p–n junction [37]. After measurement of one component of the data, the Kramers–Kronig transformations can be employed to construct the other, although since frequencies are never truly measured from 0 to ∞ this is done with the assistance of approximations or fits to the data [38, 39]. Particularly in electrochemical measurements, it is common to use this procedure to verify the conductance measurement, but such tests are not necessarily definitive [40].

While the G/ω peaks can be a good way to observe the position of the capacitance step, they can be masked by the leakage conductance in some samples; analogous peaks can also be obtained from the derivative

$$\frac{dC}{dE_e} = -\frac{\omega}{kT}\frac{dC}{d\omega} \tag{4.12}$$

as illustrated in Figure 4.6b. The (ω, T) data points from each peak can then be plotted on an Arrhenius plot; typically $\ln(\omega/T^2)$ is graphed as a function of $1000/T$ as shown in Figure 4.6c. Using Eq. (4.2), the slope then yields the apparent activation energy E_{na}, while the intercept gives the apparent capture cross section σ_{na}. These quantities may differ from the trap energy and the trap capture cross section, as discussed above in Section 4.6. The graph of $\omega dC/d\omega$ versus ω can be transformed into $N_t(E_e)$ versus E_e by using the measured σ_{na} to rescale the ω axis to E_e, and calculating $N_t(E)$ according to [38]

$$N_t(E_e) \approx -\frac{V_{bi}^2}{W[eV_{bi}-(E_{F\infty}-E_e)]}\frac{\omega}{kT}\frac{dC}{d\omega} \tag{4.13}$$

where $E_{F\infty}$ indicates the position of the Fermi energy in the bulk. Rescaling of the ω axis to E_e has been illustrated in Figure 4.6d, although in that case the signal magnitude is scaled using DLCP data as described in the caption. For broad densities of states, a clear peak may not be observable in $\omega dC/d\omega$ versus ω, in which case the factor necessary to rescale the ω axis such that all of the $\omega dC/d\omega$ curves overlap can yield an estimate for σ_{na}.

The Arrhenius plot is commonly interpreted to directly yield E_T; however, in many materials the apparently same trap response has been observed with differing E_{na} and σ_{na} values. These are often related by

$$\sigma_{na} = \sigma_{00}\exp\left(\frac{E_{na}}{E_{char}}\right) \tag{4.14}$$

such that a graph of $\ln\sigma_{na}$ versus E_{na} yields a straight line with slope E_{char}^{-1} and intercept $\ln\sigma_{00}$. The quantities E_{char} and σ_{00} are phenomenologically observed parameters. This relationship is known as the Meyer–Neldel rule, and is further discussed in Section 4.12.

4.10
Drive Level Capacitance Profiling

The technique of DLCP determines the density of states responding dynamically to the ac bias. Like AS, this technique allows different trap response energies to be isolated by adjusting the temperature and frequency of the measurement. At the same time, DLCP yields a density somewhat analogous to CV; however, in DLCP, the *ac* voltage amplitude, V_{ac}, is varied to determine the density.

The value of V_{ac} employed in DLCP no longer satisfies the small signal condition, and the capacitance response, as a function of V_{ac}, is fit to yield higher order corrections

$$C = C_0 + C_1 dV + C_2 dV^2 + \cdots \tag{4.15}$$

Note that, as V_{ac} is varied, at the same time the dc bias must be adjusted so that the maximum applied voltage remains constant, that is, the voltage waveforms are aligned at their peaks [41]. This gives an accurate value for the small signal capacitance, C_0, as well as an additional experimental parameter C_1. In DLCP, the values of C_0 and C_1 are used to find the gap state density according to [44]

$$N_{DL} \equiv -\frac{C_0^3}{2e\varepsilon\varepsilon_0 A^2 C_1} = p + \int_{E_F^\infty}^{E_V + E_e} g(E, x_e)\, dE \tag{4.16}$$

for an n^+–p device, where an analogous equation can be written for a p^+–n device. In Eq. (4.16), N_{DL} is the free carrier density plus the trap density that is able to respond at E_e, and $g(E, x_e)$ is the density of states in the gap at the location x_e.

Since DLCP is a purely ac measurement, the carriers contributing to N_{DL} are exactly those responding in an AS measurement. The same activation of trap response as a function of f, T can be observed, as illustrated in Figure 4.6d. In samples with deep traps, the high-frequency DLCP can give a more accurate estimation of free carrier density than CV profiling data [23]. At low frequencies, DLCP should give the same result as CV profiling, where low frequencies are defined such that all traps that change their charge with the dc bias in CV also respond dynamically to the ac bias. DLCP gives the trap density more directly than AS, not requiring any particular knowledge about the device other than the dielectric constant.

The DLCP measurement can be repeated as a function of V_{dc}, to yield $N_{DL}(\langle x \rangle)$, with the spatial sensitivity roughly determined by the Debye length [42]. The profile $N_{DL}(\langle x \rangle)$ helps to identify spatial variations through the film [23, 43], and responses that are localized or at the interface. The issue of spatial variation is further discussed in Section 4.13.

4.11 Photocapacitance

Photocapacitance experiments come in many variations, all intended to measure the optical energy and cross section for transitions between traps and the conduction or valence band. The change in charge of the junction due to optical excitation of carriers into or out of defects results in a capacitance change that can be measured as a function of photon energy. While there is not space here to delve into the details of these measurements, we give a brief discussion of their benefits and references for further study.

Transient photocapacitance techniques allow a particular thermal transition to be clearly associated with its corresponding optical transition(s), and include both deep

level optical spectroscopy (DLOS) [44] and transient photocapacitance spectroscopy (TPC) [45], which are based on the technique of DLTS. Essentially the DLTS experimental setup can be used, with the addition of a monochromatic light source, filters, and a shutter to control optical excitation of the sample. In these measurements, voltage or optical filling pulses are employed to alter trap occupation from its equilibrium value. The ensuing transient is observed under monochromatic optical excitation.

In DLOS, the transient rate is measured at times as close as possible to time = 0 (measured from the end of the filling pulse) to isolate the optically induced excitation of carriers out of the traps from the thermal relaxation. In TPC, transients in the light and in the dark are subtracted to remove the thermal part of the relaxation from the signal. The TPC technique utilizes a very low light intensity, selected such that the signal varies linearly with photon flux.

In both cases, the temperature and filling pulse are chosen carefully from either DLTS or AS data such that the optical response associated with particular thermal transients can be isolated. For example, following a majority carrier filling pulse, at high temperatures a trap may thermally empty very rapidly, more quickly than the response time of the electronics. At a lower temperature, the same trap may have a time constant on the order of seconds, such that it is not significantly thermally emptied during the time scale of the measurement. Only in the latter case could the trap contribute to the optically induced aspect of the transient. By subtracting the high and low temperature spectra, the optical transition(s) associated with a specific defect, which has already been observed thermally, may be identified.

In some cases, dramatically different optical and thermal energies have been observed, allowing a better understanding of the lattice relaxation associated with changes in occupation of a trap; the DX centers in GaAs are a well-known example [46].

These techniques allow what is essentially an optical absorption spectrum of the buried absorber layer in the complete, working device to be measured. Since many characteristics of the film can be altered due to deposition of ensuing layers (such as due to high temperatures, migration of elements, etc.), this can be a valuable tool, for example, to study the role of Ga and Na in CIGS [47, 48].

Finally, a similar measurement can be conducted while measuring the current, rather than capacitance, response of the device. This technique, dubbed transient photocurrent spectroscopy, gives complementary information to TPC. This is because the capacitance response depends on net charge change, p–n, in the device, while the current transient shows the total carriers excited out of the traps, p+n. The difference between these spectra can be used to better understand minority carrier transport in the film [49].

4.12
The Meyer–Neldel Rule

The Meyer–Neldel rule is a very general rule describing thermally activated processes for which the measured prefactors and energies in different samples are interrelated

by Eq. (4.14). Meyer and Neldel observed that the activated dc conductivity of several related oxide semiconductors followed this relationship [50]. Since that time, many thermally activated processes have been observed to follow the Meyer–Neldel rule. In a-Si:H, it is observed in such seemingly disparate processes as the thermal annealing of defects and the activation of dc conductivity [51, 52]; AS spectroscopy data for CIGS are discussed in Ref. [53]. The Meyer–Neldel rule is also known as the compensation rule when it is observed in thermally activated rate processes of chemical reactions (see, for example, Ref. [54]).

The Eyring model, essentially the recognition that the measured transition corresponds to an increase in Gibbs free enthalpy, ΔG, for the thermodynamic system upon ionization, is the most generally accepted explanation of this behavior [55]. The trap energy is $E_T - E_V = \Delta G$ (for an acceptor-type trap). But, since ΔG is separated into entropy, ΔS, and enthalpy, ΔH, terms by $\Delta G = \Delta H - T\Delta S$ the measured thermal activation energy corresponds to ΔH rather than ΔG, and the value of ΔS affects the apparent capture cross section.

Then, Eq. (4.2) becomes

$$e_n = \gamma_n N_c \sigma_n \langle v_n \rangle \frac{g_0}{g_1} \exp\left(-\frac{\Delta H}{kT}\right)$$

where

$$\gamma_n = \exp\left(\frac{\Delta S}{k}\right)$$

For deep states, ΔS is thought to predominantly originate from the change in lattice vibrations occurring with the change in occupancy, and bonding configuration, of the defect. A discussion of ΔS for traps in CIGS is given in [15]. When the electronic transition does not involve phonons, the localized state is not coupled to the local phonon modes, and the electronic degeneracy is neglected, then it has been shown that $\Delta S = 0$ and $\Delta G = \Delta H$ [56]. This includes transitions from the shallow, hydrogenic dopant states.

Explanations attempting to quantify ΔS and relate it to conduction in semiconductors focus on the electron–phonon interaction [57–59]. Unrelated mechanisms can cause apparent Meyer–Neldel behavior, especially when trends are only observed over one or two orders of magnitude. For example, see Refs. [60, 61].

4.13
Spatial Inhomogeneities and Interface States

In thin-film solar cell materials, spatial inhomogeneities and interface states are often present. Here we consider only inhomogeneities through the depth of the film. Inhomogeneity could be observed in N_T, E_{na}, σ_{na}, or all of these. Since changes in band bending or E_F affect x_e, most of the techniques discussed here may probe a range of trap locations over the course of the measurement, and inhomogeneity will

lead to anomalous results. One exception is DLCP, in which the trap density can be measured by varying only the frequency, keeping T and V_{dc} constant (even so, the trap response and free carrier response occur at two different locations in the film, and the spatial resolution is limited).

In most cases it is possible to test a hypothesis of inhomogeneity in AS by repeating the measurement at a different value of V_{dc}. For a uniform sample, λ should remain constant with dc bias. So, $\langle x_H\rangle - \langle x_L\rangle = \varepsilon\varepsilon_0 A\left(C_H^{-1} - C_L^{-1}\right)$ should not vary with V_{dc}, where C_H and C_L correspond to measurements above and below the transition frequency for the trap, respectively. However, this same identity could also hold true for an interface minority carrier trap or for a double-diode device with a nonohmic back contact, as discussed below.

An extremely important issue in thin-film photovoltaic devices are interface states, which represent a special case of inhomogeneity. The characteristic energy at which interface states respond dynamically to the ac bias corresponds to the Fermi energy at the interface. Assuming that E_F is not pinned at the interface, and that the density of interface states $N_I(E)$ is spread fairly uniformly over a wide range of energies, then the apparent activation energy of interface states will shift with V_{dc} (and possibly T); such a measurement also allows $N_I(E)$ to be profiled. These characteristics, particularly a shift of E_{na} with V_{dc}, are highly suggestive of near-interface traps [8] (but not to be confused with freeze-out of the mobility, which can also be bias dependent [39]).

A spatially and energetically localized density of states (including near the interface) could appear as a peak in N_{CV} occurring at a particular value of V_{dc}, because W changes abruptly with V_{dc} as the trap state crosses from above to below E_F; such a peak should generally be suppressed in DLCP except at the exact T and f at which the trap state can respond to the ac voltage [46]. Hence, comparisons of results between different parameter values and different techniques can be extremely useful.

It is also possible for an interface minority carrier trap to be filled and emptied via the highly doped side of the junction. The barrier height for such a response may remain roughly constant with V_{dc}, since there is not a large potential drop on the highly doped side of the interface. This situation would appear like a bulk trap, where $\langle x_H\rangle - \langle x_L\rangle = \varepsilon\varepsilon_0 A\left(C_H^{-1} - C_L^{-1}\right)$ is constant with V_{dc} [21, 62]. In some cases the two possibilities can be distinguished by the magnitude of $\langle x_H\rangle - \langle x_L\rangle$, which, in the case of an interface trap, will correspond to the relatively small depletion width on the highly doped side of the interface plus the thickness of any intrinsic buffer layer at the interface. Otherwise, variations in the sample preparation, such as replacement of the one-sided junction with a Schottky junction, are necessary to resolve this question.

Such a study has indeed yielded new information on a long-discussed trap in CIGS, showing that the trap response remains even in Schottky devices and indicating instead that the measured response could originate from a nonohmic back contact, which would give a similar C–V result [63]. In this case, the activation energy corresponds to the back contact barrier height. The presence of a nonohmic back contact may be identifiable from I–V–T measurements [64, 65].

In principle, DLTS is much less sensitive for charge changes taking place in the vicinity of the interface. However, both majority and minority carrier traps at the interface can be effectively investigated by DLTS in MIS-like structures, as already

indicated. This requires some modifications from the standard DLTS measurement discussed above, and in particular, the pulse amplitude must be carefully chosen. The investigation of interface states in MIS structures by DLTS was discussed extensively by Murray *et al*. [28].

4.14 Metastability

An additional complication occurs when sample properties can be persistently changed by external factors like voltage stress or illumination, and then recovered, perhaps after heating the sample in a controlled environment and in the dark. In practice, such effects are common, but the details are characteristic to each specific material, and indeed may depend on aspects of device preparation that are closely, but not identically, duplicated in different laboratories. Thus it is critical to carefully control the sample environment until its sensitivities are understood, and to check for repeatability of measurements. Unfortunately, metastable effects may be observed under the conditions necessary for capacitance spectroscopy measurements, which then necessitates careful, and sometimes laborious, experimental procedures. An introduction to these issues for some common solar cell materials can be found in [29, 51, 66–73].

References

1 Feichtinger, H. (1991) Deep centers in semiconductors, in *Electronic Structure and Properties of Semiconductors* (ed. W. Schröter), VCH Publishers, New York, pp. 143–195.

2 Losee, D.L. (1975) Admittance spectroscopy of impurity levels in Schottky barriers. *J. Appl. Phys.*, **46**, 2204.

3 Lang, D.V., Cohen, J.D., and Harbison, J.P. (1982) Measurement of the density of gap states in hydrogenated amorphous silicon by space charge spectroscopy. *Phys. Rev. B*, **25**, 5285.

4 Cohen, J.D. and Lang, D.V. (1982) Calculation of the dynamic response of Schottky barriers with a continuous distribution of gap states. *Phys. Rev. B*, **25**, 5321.

5 Blood, P. and Orton, J.W. (1992) *The Electrical Characterization of Semiconductors: Majority Carriers and Electron States*, Academic Press, San Diego.

6 Schroeder, D.K. (2006) *Semiconductor Material and Device Characterization*, John Wiley and Sons, Inc., Hoboken, NJ.

7 Jonscher, A.K. (1983) *Dielectric Relaxation in Solids*, Chelsea Dielectrics Press, Ltd, Chelsea.

8 Nicollian, E.H. and Brews, J.R. (1982) *MOS (Metal Oxide Semiconductor) Physics and Technology*, Wiley, New York, USA.

9 Istratov, A.A. and Vyvenko, O.F. (1999) Exponential analysis in physical phenomena. *Rev. Sci. Instrum.*, **70**, 1233.

10 Callegaro, L. (2009) The metrology of electrical impedance at high frequency: A review. *Meas. Sci. Technol.*, **20**, 022002.

11 Sze, S.M. (1985) *Semiconductor Devices Physics and Technology*, John Wiley & Sons, Inc., New York.

12 Hilibrand, J. and Gold, R.D. (1960) Determination of the impurity distribution in junction diodes from

capacitance–voltage measurements. *RCA Rev.*, **21**, 245.
13 Johnson, W.C. and Panousis, P.T. (1971) The influence of Debye length on the C–V measurement of doping profiles. *IEEE Trans. Electron. Devices*, **ED-18**, 965.
14 Crandall, R.S. (1980) Trap spectroscopy of a-Si:H diodes using transient current techniques. *J. Electron. Mater.*, **9**, 713.
15 Young, D.L. and Crandall, R.S. (2005) Strongly temperature-dependent free energy barriers measured in a polycrystalline semiconductor. *Appl. Phys. Lett.*, **86**, 262107.
16 Branz, H.M. (1988) Charge-trapping model of metastability in doped hydrogenated amorphous silicon. *Phys. Rev. B*, **38**, 7475.
17 Branz, H.M. and Crandall, R.S. (1989) Ionization entropy and charge-state-controlled metastable defects in semiconductors. *Appl. Phys. Lett.*, **55**, 2634.
18 Los, A.V. and Mazzola, M.S. (2001) Semiconductor impurity parameter determination from Schottky junction thermal admittance spectroscopy. *J. Appl. Phys.*, **89**, 3999.
19 Los, A.V. and Mazzola, M.S. (2002) Model of Schottky junction admittance taking into account incomplete impurity ionization and large signal effects. *Phys. Rev. B*, **65**, 165319.
20 Burgelman, M., Nollet, P., and Degrave, S. (2000) Modelling polycrystalline semiconductor solar cells. *Thin Solid Films*, **361–362**, 527.
21 Ćwil, M., Igalson, M., Zabierowski, P., and Siebentritt, S. (2008) Charge and doping distributions by capacitance profiling in Cu(In,Ga)Se_2 solar cells. *J. Appl. Phys.*, **103**, 063701.
22 Kimmerling, L.C. (1974) Influence of deep traps on the measurement of free-carrier distributions in semiconductors by junction capacitance techniques. *J. Appl. Phys.*, **45**, 1839.
23 Heath, J.T., Cohen, J.D., and Shafarman, W.N. (2004) Bulk and metastable defects in $CuIn_{1-x}Ga_xSe_2$ thin films using drive-level capacitance profiling. *J. Appl. Phys.*, **95**, 1000.
24 Lang, D.V. (1974) Deep-level transient spectroscopy: A new method to characterize traps in semiconductors. *J. Appl. Phys.*, **45**, 3023.
25 Johnston, S.W., Kurtz, S., Friedman, D.J., Ptak, A.J., Ahrenkiel, R.K., and Crandall, R.S. (2005) Observed trapping of minority-carrier electrons in p-type GaAsN during deep-level transient spectroscopy. *Appl. Phys. Lett.*, **86**, 072109.
26 Kurtz, S., Johnston, S., and Branz, H.M. (2005) Capacitance-spectroscopy identification of a key defect in N-degraded GaInNAs solar cells. *Appl. Phys. Lett.*, **86**, 113506.
27 Kukimoto, H., Henry, C.H., and Merritt, F.R. (1973) Photocapacitance studies of the oxygen donor in GaP. I. Optical cross-sections, energy levels, and concentration. *Phys. Rev. B*, **7**, 2486.
28 Murray, F., Carìn, R., and Bogdanski, P. (1986) Determination of high-density interface state parameters in metal-insulator-semiconductor structures by deep-level transient spectroscopy. *J. Appl. Phys.*, **60**, 3592.
29 Zabierowski, P. Electrical characterization of CIGSe-based thin film photovoltaic devices, in *Thin Film Solar Cells: Current Status and Future Trends* (eds A. Romeo and A. Bossio), Nova Science Publishers, Hauppauge, NY.
30 For an example of an exception, see: Grillot, P.N., Ringel, S.A., Fitzgerald, E.A., Watson, G.P., Xie, Y.H. (1995) Minority- and majority-carrier trapping in strain-relaxed $Ge_{0.3}Si_{0.7}$/Si heterostructure diodes grown by rapid thermal chemical-vapor deposition. *J. Appl. Phys.*, **77**, 676.
31 Look, D.C. and Sizelove, J.R. (1995) Depletion width and capacitance transient formulas for deep traps of high concentration. *J. Appl. Phys.*, **78**, 2848.
32 Buchwald, W.R., Morath, C.P., and Drevinsky, P.J. (2007) Effects of deep defect concentration on junction space charge capacitance measurements. *J. Appl. Phys.*, **101**, 094503.
33 Frenkel, J. (1938) On pre-breakdown phenomena in insulators and electronic semiconductors. *Phys. Rev.*, **54**, 647.

34 Vincent, G., Chantre, A., and Bois, D. (1979) Electric field effect on the thermal emission of traps in semiconductor junctions. *J. Appl. Phys.*, **50**, 5484.

35 Li, G.P. and andWang, K.L. (1985) Detection sensitivity and spatial resolution of reverse-bias pulsed deep-level transient spectroscopy for studying electric field-enhanced carrier emission. *J. Appl. Phys.*, **57**, 1016.

36 Dobaczewski, L., Peaker, A.R., and Bonde Nielsen, K. (2004) Laplace-transform deep-level spectroscopy: The technique and its applications to the study of point defects in semiconductors. *J. Appl. Phys.*, **96**, 4689.

37 Zabierowski, P. and Edoff, M. (2005) Laplace-DLTS analysis of the minority carrier traps in the $Cu(In,Ga)Se_2$-based solar cells. *Thin Solid Films*, **480–481**, 301.

38 Walter, T., Herberholz, R., Müller, C., and Schock, H.W. (1996) Determination of defect distributions from admittance measurements and application to $Cu(In,Ga)Se_2$ based heterojunctions. *J. Appl. Phys.*, **80**, 4411.

39 Lee, J.W., Cohen, J.D., and Shafarman, W.N. (2005) The determination of carrier mobilities in CIGS photovoltaic devices using high-frequency admittance measurements. *Thin Solid Films*, **480**, 336.

40 Dhariwal, S.R. and Deoraj, B.M. (1992) Contribution of bulk states to the depletion layer admittance. *Solid State Electron.*, **36**, 1165.

41 León, C., Martin, J.M., Santamaría, J., Skarp, J., González-Díaz, G., and Sánchez-Quesada, F. (1996) Use of Kramers–Kronig transforms for the treatment of admittance spectroscopy data of p–n junctions containing traps. *J. Appl. Phys.*, **79**, 7830.

42 Milton, G.W., Eyre, D.J., and Mantese, J.V. (1997) Finite frequency range Kramers–Kronig relations: Bounds on the dispersion. *Phys. Rev. Lett.*, **79**, 3062.

43 van de Leur, R.H.M. (1991) A critical consideration on the interpretation of impedance plots. *J. Phys. D Appl. Phys.*, **24**, 1430.

44 Michelson, C.E., Gelatos, A.V., and Cohen, J.D. (1985) Drive-level capacitance profiling: Its application to determining gap state densities in hydrogenated amorphous silicon films. *Appl. Phys. Lett.*, **47**, 412.

45 Unold, T. and Cohen, J.D. (1991) Enhancement of light-induced degredation in hydrogenated amorphous silicon due to carbon impurities. *Appl. Phys. Lett.*, **58**, 723.

46 Johnson, P.K., Heath, J.T., Cohen, J.D., Ramanathan, K., and Sites, J.R. (2005) A comparative study of defect states in selenized and evaporated CIGS(S) solar cells. *Prog. Photovoltaics*, **13**, 1.

47 Chantre, A., Vincent, G., and Bois, D. (1981) Deep-level optical spectroscopy in GaAs. *Phys. Rev. B*, **23**, 5335.

48 Cohen, J.D. and Gelatos, A.V. (1988) Transient photocapacitance studies of deep defect transitions in hydrogenated amorphous silicon, in *Amorphous Silicon and Related Materials Vol. A* (ed. H. Fritzsche), World Scientific Publishing, Singapore, pp. 475–512.

49 Lang, D. (1992) DX centers in III-V alloys, in *Deep Centers in Semiconductors A State-of-the-Art Approach*, 2nd edn (ed. S.T. Pantelides), Gordon and Breach Science Publishers, Yverdon, Switzerland, pp. 592–665.

50 Heath, J.T., Cohen, J.D., Shafarman, W.N., Liao, D.X., and Rockett, A.A. (2002) Effect of Ga content on defect states in $CuIn_{1-x}Ga_xSe_2$ photovoltaic devices. *Appl. Phys. Lett.*, **80**, 4540.

51 Erslev, P.T., Lee, J.W., Shafarman, W.N., and Cohen, J.D. (2009) The influence of Na on metastable defect kinetics in CIGS devices. *Thin Solid Films*, **517**, 2277.

52 Cohen, J.D., Unold, T., Gelatos, A.V., and Fortmann, C.M. (1992) Deep defect structure and carrier dynamics in amorphous silicon and silicon–germanium alloys determined by transient photocapacitance methods. *J. Non-Cryst. Solids*, **141**, 142.

53 Meyer, W. and Neldel, H. (1937) Über die Beziehungen zwischen der Energiekonstanten und der Mengenkonstanten *a* in der Leitwerts-Temperaturformel bei oxydischen

Halbleitern. *Zeitschrift für technische Physik*, **12**, 588.
54 Street, R.A. (1991) *Hydrogenated Amorphous Silicon*, Cambridge University Press, Cambridge, p. 224.
55 Crandall, R.S. (1990) Defect relaxation in amorphous silicon: Stretched exponentials, the Meyer–Neldel rule, and the Staebler–Wronski effect. *Phys. Rev. B*, **43**, 4057.
56 Herberholz, R., Walter, T., Müller, C., Friedlmeier, T., Schock, H.W., Saad, M., Lux-Steiner, M.Ch., and Albertz, V. (1996) Meyer–Neldel behavior of deep level parameters in heterojunctions to Cu(In, Ga)(S,Se)$_2$. *Appl. Phys. Lett.*, **69**, 2888.
57 Leffler, J.E. (1955) The enthalpy–entropy relationship and its implications for organic chemistry. *J. Org. Chem.*, **20**, 1202.
58 Glasstone, S., Laidler, K.J., and Eyring, H. (1941) *The Theory of Rate Processes*, McGraw-Hill, New York.
59 Almbladh, C.O. and Reese, G.J. (1982) Statistical mechanics of electronic energy levels in semiconductors. *Solid State Commun.*, **41**, 173.
60 Engström, O. and Alm, A. (1978) Thermodynamical analysis of optimal recombination centers in thyristors. *Solid State Electron.*, **21**, 1571.
61 Yelon, A. and Movaghar, B. (1990) Microscopic explanation of the compensation (Meyer–Neldel) rule. *Phys. Rev. Lett.*, **65**, 618.
62 Yelon, A., Movaghar, B., and Branz, H.M. (1992) Origin and consequences of the compensation (Meyer–Neldel) law. *Phys. Rev. B*, **46**, 12244; Viščor, P. (2002) Comment on "Origin and consequences of the compensation (Meyer–Neldel) law". *Phys. Rev. B*, **65**, 077201; Yelon, A. and Movaghar, B. (2002) Reply to "Comment on 'Origin and consequences of the compensation (Meyer–Neldel) law'". *Phys. Rev. B*, **65**, 077202.
63 Widenhorn, R., Rest, A., and Bodegom, E. (2002) The Meyer–Neldel rule for a property determined by two transport mechanisms. *J. Appl. Phys.*, **91**, 6524.
64 Popescu, C. and Stoica, T. (1992) Meyer–Neldel correlation in semiconductors and Mott's minimum metallic conductivity. *Phys. Rev. B*, **46**, 15063.
65 Niemegers, A., Burgelman, M., Herberholz, R., Rau, U., Hariskos, D., and Schock, H.W. (1998) Model for electronic transport in Cu(In,Ga)Se$_2$ solar cells. *Progr. Photovoltaics: Res. Appl.*, **6**, 407.
66 Eisenbarth, T., Unold, T., Caballero, R., Kaufmann, C.A., and Schock, H.-W. (2010) Interpretation of admittance, capacitance–voltage, and current–voltage signatures in Cu(In,Ga)Se$_2$ thin film solar cells. *J. Appl. Phys.*, **107**, 034509.
67 Niemegeers, A. and Burgelman, M. (1997) Effects of the Au/CdTe back contact on IV and CV characteristics of Au/CdTe/CdS/TCO solar cells. *J. Appl. Phys.*, **81**, 2881.
68 Demtsu, S.H. and Sites, J.R. (2006) Effect of back-contact barrier on thin-film CdTe solar cells. *Thin Solid Films*, **510**, 320.
69 Macdonald, D., Rougieux, F., Cuevas, A., Lim, B., Schmidt, J., Di Sabatino, M., and Geerligs, L.J. (2009) Light-induced boron–oxygen defect generation in compensated p-type Czochralski silicon. *J. Appl. Phys.*, **105**, 093704.
70 Nadazdy, V. and Zeman, M. (2004) Origin of charged gap states in a-Si:H and their evolution during light soaking. *Phys. Rev. B*, **69**, 165213.
71 Shimizu, T. (2004) Staebler–Wronski effect in hydrogenated amorphous silicon and related alloy films. *Jpn. J. Appl. Phys.*, **43**, 3257.
72 Balcioglu, A., Ahrenkiel, R.K., and Hasoon, F. (2000) Deep-level impurities in CdTe/CdS thin-film solar cells. *J. Appl. Phys.*, **88**, 7176.
73 Demtsu, S.H., Albin, D.S., Pankow, J.W., and Davies, A. (2006) Stability study of CdS/CdTe solar cells made with Ag and Ni back-contacts. *Sol. Energy Mater. Sol. C*, **90**, 2934.